

Unsupervised Representation Learning for 3D MRI Super Resolution with Degradation Adaptation

Jianan Liu [#], Hao Li [#], Tao Huang, Euijoon Ahn, Adeel Razi, Wei Xiang

arXiv:2205.06891v1 [eess.IV] 13 May 2022

Abstract— High-resolution (HR) MRI is critical in assisting the doctor’s diagnosis and image-guided treatment, but is hard to obtain in a clinical settings due to long acquisition time. Therefore, the research community investigated deep learning-based super-resolution (SR) technology to reconstruct HR MRI images with shortened acquisition time. However, training such neural networks usually requires paired HR and low-resolution (LR) in-vivo images, which are difficult to acquire due to patient movement during and between the image acquisition. Rigid movements of hard tissues can be corrected with image-registration, whereas the alignment of deformed soft tissues is challenging, making it impractical to train the neural network with such authentic HR and LR image pairs. Therefore, most of the previous studies proposed SR reconstruction by employing authentic HR images and synthetic LR images downsampled from the HR images, yet the difference in degradation representations between synthetic and authentic LR images suppresses the performance of SR reconstruction from authentic LR images. To mitigate the aforementioned problems, we propose a novel Unsupervised DEgradation Adaptation Network (UDEAN). Our model consists of two components: the degradation learning network and the SR reconstruction network. The degradation learning network downsamples the HR images by addressing the degradation representation of the misaligned or unpaired LR images, and the SR reconstruction network learns the mapping from the downsampled HR images to their original HR images. As a result, the SR reconstruction network can generate SR images from the LR images and achieve comparable quality to the HR images. Experimental results show that our method outperforms the state of the art models and can potentially be applied in real-world clinical settings.

Index Terms— 3D MRI, Super Resolution, Unsupervised Learning, Representation Learning, Geometric Deformation, Degradation Adaptation, Clinical Setting.

I. INTRODUCTION

[#] Jianan Liu and Hao Li contribute equally to the work and are co-first authors.

Jianan Liu is with Vitalent Consulting, Gothenburg, Sweden, and Silo AI, Stockholm, Sweden.

Hao Li is with Department of Neuroradiology, University Hospital Heidelberg, Heidelberg, Germany.

Tao Huang and Euijoon Ahn are with College of Science and Engineering, James Cook University, Cairns, Australia.

Adeel Razi is with Turner Institute for Brain and Mental Health, School of Psychological Sciences, Monash University, Melbourne, Australia.

Wei Xiang is with School of Computing, Engineering and Mathematical Sciences, La Trobe University, Melbourne, Australia.

HIGH resolution (HR) MRI provides abundant soft tissue contrast and detailed anatomical structures, which assist doctors on accurate diagnosis and image-guided treatment. However, higher resolution results in longer acquisition time. Therefore, deep learning based SR reconstruction technology has been proposed to accelerate the MRI acquisition in recent years [1]–[4]. Most of these studies are based on supervised learning [1]–[7], [15]. Ideally, when training such a neural network, one can use paired LR and HR MRI images from the same scan session. However, the misalignment is introduced to the HR and LR MRI image pair due to patient movement during and between the image acquisition. The misalignment incurs significant errors in the SR MRI image generation, making it unusable in actual clinical practice.

A straightforward solution is to estimate the transformation between misaligned authentic HR and authentic LR images by image-registration [15]. Yet image-registration only works for rigid movement of hard tissues, the non-rigid geometric deformation caused by soft tissues movement is hardly handled [16]. Another solution is training the network using authentic HR images and synthetic LR images which are downsampled by using a deterministic downsampling filter (e.g. Gaussian blur filter) or K -space truncation from the authentic HR images [1]–[7]. The authentic LR images are then fed in a trained network to reconstruct SR images. Most of previous works in MRI SR reconstruction follows this routine with designing different network models: Both DCSRN [2] and CSN [4] utilize DenseNet [25] to enhance the feature fusion for the reconstruction procedure; mDCSRN [3], as the extension of DCSRN, increases the depth of SR reconstruction network and applies discriminator to facilitate its capability; the authors of [5] incorporates the spatial gradient of LR images as prior to guide the MRI SR reconstruction; SERAN [6] employs attention mechanism into MRI SR reconstruction procedure; and leveraging of HR reference from another modality as prior information is also introduced on top of attention based network in MINet [7] to achieve outstanding performance. Besides, TS-RCAN [8] achieves the slightly better performance compare to MINet with only single modality data and great reduction of demands on computational resource and inference time.

However, it is worth pointing out that the deterministic downsampling filters are widely used in computer vision tasks but do not fit MR image acquisition. The K -space

truncation is based on the assumption that authentic HR and authentic LR images are fully sampled, whereas, in actual clinical settings, they are acquired with acceleration techniques including partial Fourier, elliptical K -space, etc., thus the K -space truncation can not represent the actual degradation process from authentic HR images to authentic LR images well. As a result, such difference between the real degradation process from authentic HR images to authentic LR images and degradation process using K -space truncation from authentic HR images to synthetic LR images leads to the existence of degradation shift, thus obtaining poor performance of MRI SR reconstruction.

Several unsupervised SR approaches which have been proposed in generic computer vision area by only employing the unpaired LR and HR images for training, might be possible to avoid such degradation shift in the supervised MRI SR reconstruction procedure mentioned above. ZSSR [9] learns the degradation from LR image to LR image with lower resolution and utilizes such learnt degradation to fit the inverse process from LR image to HR image, HR-Ref-ZSSR [10] chooses to apply such procedure to MRI image SR with HR reference provided from another modality, ZSSR-GAN [11] implements the similar idea by augmenting the network with discriminator. Nevertheless, above approaches still suffer by the degradation shift caused by the inconsistency between learnt degradation from LR image to LR image with lower resolution and the degradation from HR image to LR image.

Such degradation shift might be mitigated by the applying an approach originally designed for transferring the style from one domain to another, such as CycleGAN [12], where source domain and target domains are defined and the images can be transferred between the two domains. Pseudo-SR [13] transfers the target domain LR image to the source domain using the CycleGAN framework, and then uses an SR network to reconstruct SR image in the source domain. Nonetheless, these CycleGAN-based approaches only transfer the domain information in the image space rather than latent feature space. DASR [14], as the state-of-the-art unsupervised learning method, adapts the image domain information in two steps. It firstly calculates a domain distance map besides of transferring source domain HR image to target domain LR image using a downsampling network. And then, using loss functions guided by the domain distance map, it trains an SR network to transfer the target domain LR picture back to the source domain HR image. However, with no end-to-end training, the model is unlikely to be optimally trained. Furthermore, all of these domain transfer algorithms are intended for general computer vision SR tasks and are not especially appropriate for MRI SR reconstruction.

To address the issues that unavailability of paired MRI HR and LR images and existence of degradation shift between real degradation process and K -space truncation, we propose an unsupervised learning framework which employs either misaligned or unpaired MRI HR and LR images to train the network. The contributions of this work is summarized as below:

- 1) We propose an end-to-end unsupervised degradation adaptation deep neural network UDEAN, which adap-

tively learns the degradation representation between the misaligned or unpaired authentic LR and HR MRI images in both the image space and the latent feature space, thus providing the minimized errors in the reconstructed SR MRI images.

- 2) Our proposed method can be trained with either misaligned or unpaired authentic LR and HR MRI images. Thus such a method can be applied in real clinical setting, where paired authentic LR and HR MRI images are not available.
- 3) Experimental results show that our proposed method has advantages over both existing paired supervised and unpaired unsupervised MRI SR training solutions.

II. METHODOLOGY

In this section, we introduce the factors that induces degradation shift between the real degradation process and K -space truncation, and the detailed design of UDEAN. UDEAN is an unsupervised SR model designed to resolve the SR reconstruction in a practical clinical environment where the paired authentic HR and LR MRI images are unavailable, as only **misaligned** or **unpaired** HR and LR images are required for training. For the **misaligned** training data, each HR and LR image pair was from the same patients, but spatially misaligned; for the **unpaired** training data, the HR and LR images were from different patients. Detailed data preparation is also introduced in this section.

A. Network Architecture of UDEAN

Fig.1 shows the architecture of the proposed UDEAN framework. The framework contains two components: a degradation learning network and an SR reconstruction network. There are two modules in the degradation learning network. The first module is a degradation mapping module, colored in orange as shown in Fig.1. This module contains a downsampling feature extractor and an LR decoder. The second module is an identification module consisting of an LR discriminator and a feature discriminator, as shown in Fig.1 in blue color. The SR reconstruction network includes an LR encoder and an SR decoder (colored in green), and is expected to reconstruct SR images with comparable image quality with the HR images of the source group from the LR images of the target group.

During the training step, only the **misaligned** or **unpaired** HR MRI image \mathbf{Y}_s in the source group and LR MRI image \mathbf{X}_t in the target group are used. Noting that misaligned LR and HR image can be considered as a special case of unpaired data, where the LR image contains more similar structural and content information as HR image, but the training is still not applicable in supervised manner.

As indicated along the red solid line, \mathbf{Y}_s is fed to a learnable downsampling feature extractor to extract the downsampled feature map f_s of source group. Such a feature map contains a generic degradation representation from HR to LR images. The LR decoder remaps the feature map into an LR image $X_{s \sim t}$ which contains comparable degradation representation of the target group LR image \mathbf{X}_t . Then the feature map $f_{s \sim t}$ of $X_{s \sim t}$ is extracted using an LR encoder and generates the SR

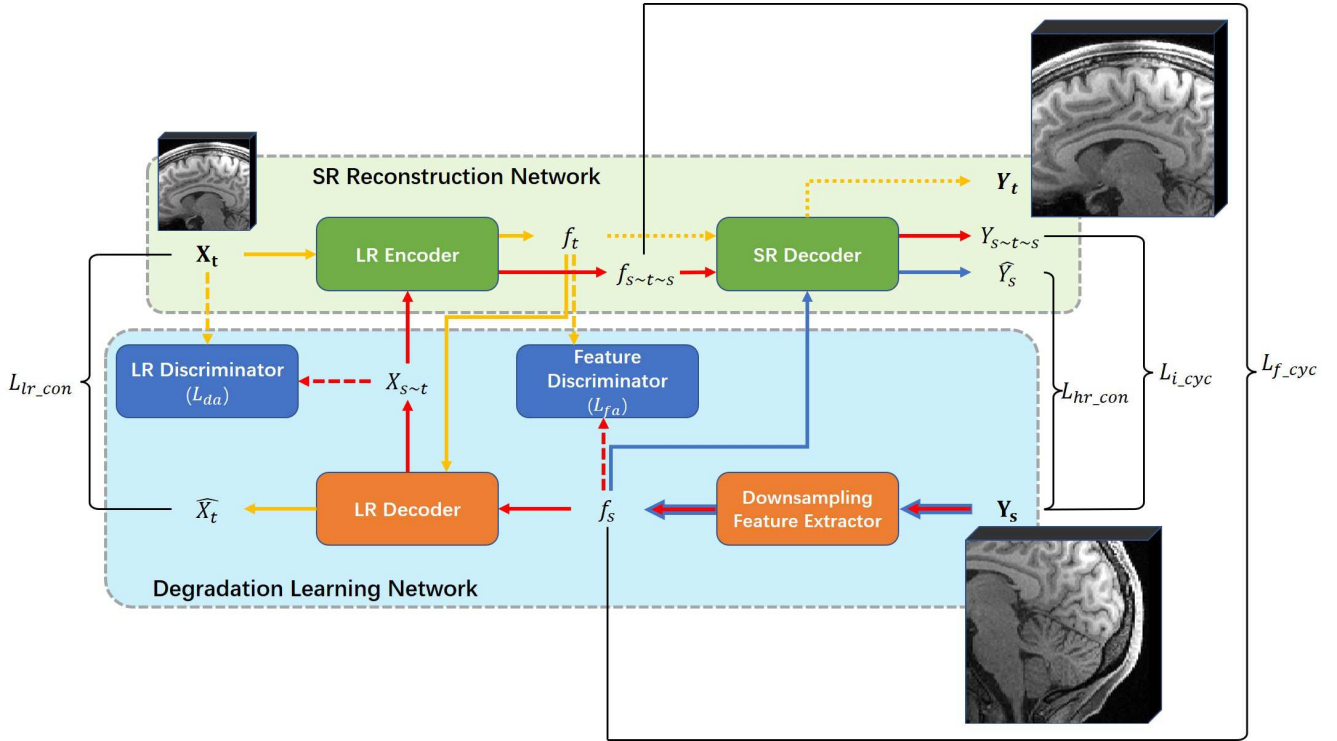


Fig. 1: The Pipeline of the Proposed UDEAN for 3D MRI Super-Resolution. The network is fed with the source group HR image patch \mathbf{Y}_s and the target group LR image patch \mathbf{X}_t in the training. During the inference, only the target group LR image patch \mathbf{X}_t is fed in the network and the SR image patch \mathbf{Y}_t is reconstructed.

image $Y_{s \sim t \sim s}$ using an SR decoder. As the reconstructed SR image $Y_{s \sim t \sim s}$ and HR image in source group \mathbf{Y}_s are expected to be identical, and the feature map $f_{s \sim t \sim s}$ and f_s should likewise contain comparable context, two cycle losses are calculated for such purposes. Two consistency losses are also involved to make the training more stable. The LR encoder and LR decoder are trained by minimizing the target group error between \mathbf{X}_t and the LR image \hat{X}_t decoded from f_t along the yellow solid line. Similarly, the downsampling feature extractor and SR decoder are trained by minimizing the source group error between \mathbf{Y}_s and SR image \hat{Y}_s reconstructed from f_s along the blue solid line.

Since the network is expected to learn the specific degradation representation from the HR images in the source group to the LR images in the target group, a LR discriminator and a feature discriminator are employed. The former is trained to distinguish between the target group LR image \mathbf{X}_t and the LR image $X_{s \sim t}$ reconstructed from source group feature. The second discriminator is trained to distinguish between the feature f_t retrieved from the target group LR and f_s . The discriminators are trained alternately with degradation mapping module and SR reconstruction network. The UDEAN can adapt from the source group to the specific degradation representation in the target group as long as the discriminators are deceived.

During the inference step, as shown along the yellow dotted line in Fig 1, only the trained LR encoder and SR decoder are required. The target group LR MRI image \mathbf{X}_t is encoded into the feature map, then the target group SR MRI image \mathbf{Y}_t is

generated accordingly.

B. Loss Functions

In our experiments, we employed three types of loss functions, which are the L1 loss, SSIM loss [17] [24] and adversarial loss:

$$L_1(x, y) = \frac{1}{N} \sum_{i=1}^N |x - y| \quad (1)$$

$$L_{SSIM}(x, y) = \frac{1}{N} \sum_{i=1}^N |1 - SSIM(x, y)^2| \quad (2)$$

$$L_{adv}(x) = \frac{1}{N} \sum_{i=1}^N \sqrt{(D(x) - 1)^2} \quad (3)$$

where $D(\cdot)$ represents the certain discriminator. To stabilize the training procedure, we use the least square loss [18] for the adversarial loss in our model instead of the negative log-likelihood [19].

As mentioned in the previous section, the two cycle losses are used to guide the cross-domain restoration of the $Y_{s \sim t \sim s}$. The image cycle loss is calculated as a weighted sum of L1 loss and SSIM loss between $Y_{s \sim t \sim s}$ and \mathbf{Y}_s , and the adversarial loss of $Y_{s \sim t \sim s}$. The feature cycle loss is calculated as the L1 loss between $f_{s \sim t \sim s}$ and f_s :

$$L_{i_cyc} = L_1(Y_{s \sim t \sim s}, \mathbf{Y}_s) + \alpha * L_{SSIM}(Y_{s \sim t \sim s}, \mathbf{Y}_s) + \beta * L_{adv}(Y_{s \sim t \sim s}) \quad (4)$$

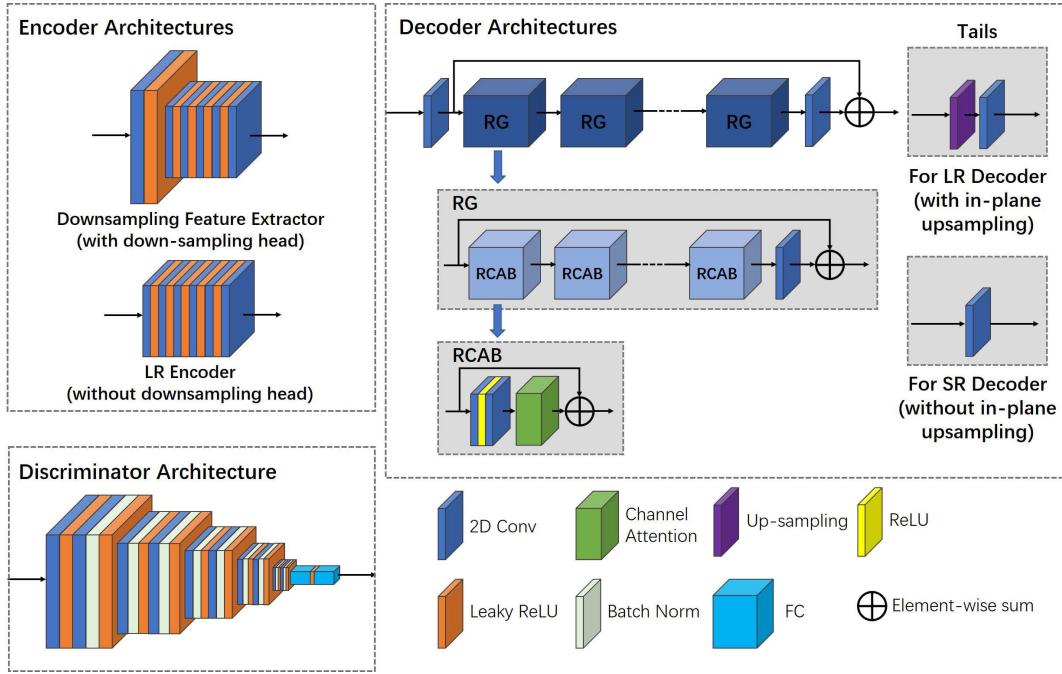


Fig. 2: Detailed Structures of Network Components.

$$L_{f_cyc} = L_1(f_{s \sim t \sim s}, f_s) \quad (5)$$

Moreover, the consistency losses are used to restrain the restoration of \hat{Y}_s and \hat{X}_t and within the source and target domain, respectively. They are calculated as a weighted sum of L1, SSIM and adversarial loss between the input and output images:

$$L_{hr_con} = L_1(\hat{Y}_s, \mathbf{Y}_s) + \alpha * L_{SSIM}(\hat{Y}_s, \mathbf{Y}_s) + \beta * L_{adv}(\hat{Y}_s) \quad (6)$$

$$L_{lr_con} = L_1(\hat{X}_t, \mathbf{X}_t) + \alpha * L_{SSIM}(\hat{X}_t, \mathbf{X}_t) + \beta * L_{adv}(\hat{X}_t) \quad (7)$$

where α and β are the weights of the SSIM and adversarial loss, respectively. We set $\alpha = 0.5$ and $\beta = 0.01$ in our experiments.

Furthermore, the degradation adaptation loss L_{da} and feature adaptation loss L_{fa} , which stem from by the LR discriminator and the feature discriminator, are used to guide the network approaching the distributions of the LR images and the features extracted from different domains:

$$L_{da}(X_{s \sim t}, \mathbf{X}_t) = \frac{1}{N} \sum_{i=1}^N |D_{da}(X_{s \sim t}) - 0.5| + \frac{1}{N} \sum_{i=1}^N |D_{da}(\mathbf{X}_t) - 0.5| \quad (8)$$

$$L_{fa}(f_t, f_s) = \frac{1}{N} \sum_{i=1}^N |D_{fa}(f_t) - 0.5| + \frac{1}{N} \sum_{i=1}^N |D_{fa}(f_s) - 0.5| \quad (9)$$

As a result, the end-to-end training loss for the generators in our network is defined as

$$Loss_G = \lambda_1 * L_{i_cyc} + \lambda_2 * L_{f_cyc} + \lambda_3 * L_{hr_con} + \lambda_4 * L_{lr_con} + \lambda_5 * L_{da} + \lambda_6 * L_{fa} \quad (10)$$

where λ_1 to λ_6 are the weights of the loss components. We set $\lambda_{1,3,4} = 1$ and $\lambda_{2,5,6} = 0.1$ in our experiments.

C. Dataset and Pre-processing

In this study, we used the T1w images from the Human Connectome Project (HCP) dataset [20], which included multi-contrast images from 1113 patients. The T1w images were acquired in the sagittal plane with 3D MPRAGE, $TR = 2400ms$, $TE = 2.14ms$, $TI = 1000ms$, $FA = 8$, $FOV = 224mm$, $rBW = 210Hz/Px$, the matrix size was $320 \times 320 \times 256$ with isotropic resolution $0.7mm$, and $\times 2$ GRAPPA in phase encoding direction was activated.

In our experiments, we involved four data groups: the source, target, validation, and test group. The source and target group were used to train the neural networks, the validation group to monitor the networks' performance during training and the test group to evaluate the networks after training. We randomly selected 120/30/30 patients from HCP dataset for the target, validation, and test group. The target group contains only LR images, which were downsampled from the HR images by 3D K -space truncation with scale factor of $2 \times 2 \times 2$. The source group contained only HR images from 120 patients, and differed between the experiments with **misaligned** and **unpaired** HR and LR images. For **unpaired** SR reconstruction, the source group contained another 120 patients which were isolated from the other three groups; For **misaligned** SR reconstruction, the source group shared the same patient group with target group, and the HR images were distorted with certain deformation pattern.

TABLE I: Numerical Comparison to Different Supervised Methods for MRI SR with Upscale Factor of $2 \times 2 \times 2$

Dataset	Method	SSIM	PSNR
HCP	TS-RCAN with misaligned LR and HR	0.8939 ± 0.0140	32.7886 ± 1.5546
	TS-RCAN with registered LR and HR	0.9025 ± 0.0116	32.7823 ± 1.5013
	TS-RCAN with degradation shift	0.9266 ± 0.0102	33.5980 ± 2.5317
	UDEAN (ours) with misaligned LR and HR	0.9247 ± 0.0097	34.2729 ± 1.8080
	UDEAN (ours) with unpaired LR and HR	0.9242 ± 0.0083	33.5159 ± 1.7234

Specifically, for the SR reconstruction from misaligned LR and HR image pairs, the patient movement between the acquisition of HR and LR images were simulated by adopting rigid movement and non-rigid geometric deformation to the HR images. The rigid movement was performed by random rotation of the image volumes by 0 to 2 degrees around the Z-axis and the X-axis (physical axes) and random translation by 0 to 2 voxels in right-left (RL) and head-feet (HF) directions. The geometric deformation was achieved by randomly shrinking the whole image volumes by 0 to 2 voxels in anterior-posterior (AP) and RL directions, resulting in 0.7 to 0.9% of change in the objects' sizes. Each dataset was scaled to the range of 0 to 1, and to save computation resource, the LR and HR images were cropped into 3D patches of sizes $64 \times 64 \times 3$ and $128 \times 128 \times 6$, respectively.

D. Implementation Details

The detailed structures of our model components are shown in Fig.2. For the encoders, we used 6 convolution layers with Leaky ReLU between each two layers, and the head layer of the downsampling feature extractor downsamples the input HR image to the same size of the LR image. We used the TS-RCAN [8] with 5 residual groups (RG) and 5 residual blocks (RCAB) in each RG as the backbone of the decoders, and VGG [23] as the discriminators for UDEAN. TS-RCAN is modified from RCAN [21] [22] to conduct 3D MRI SR task with very low consumption of computation resource and short inference time.

The networks were trained on a workstation equipped with a Nvidia Quadro A6000 graphic card. For all deep learning experiments, we used Pytorch 1.7 as the back end. In each training batch, eight LR patches were randomly extracted as inputs. We trained our model for 30 epochs using the ADAM optimizer with $\beta_1 = 0.9$, $\beta_2 = 0.99$, and $\epsilon = 10^{-8}$, and a Cosine-decay learning rate was applied from 10^{-4} to 10^{-8} . The image pre-processing of downsampling, deformation and cropping, and the post-processing and metrics calculation were performed with Matlab 2020a. The rigid image-registration were performed on Amira 3D with metrics of extended mutual information.

III. EXPERIMENTS AND RESULTS

The UDEAN was compared to other supervised methods using the data with geometric deformation, and compared to other unsupervised methods with **misaligned** and **unpaired** LR and HR MRI images.

A. Comparison with Supervised Methods

To demonstrate the negative impact from unavailability of paired MRI HR and LR images and degradation shift, and effectiveness of our proposed method, three supervised training approaches were employed as the benchmarks using TS-RCAN [8] in the supervised manner to reconstruct SR MRI images:

- 1). Benchmark 1: The TS-RCAN was trained in the supervised manner with misaligned LR and HR images directly;
- 2). Benchmark 2: The TS-RCAN was trained in the supervised manner with rigid-registered LR and HR images;
- 3). Benchmark 3: Benchmark 3: The TS-RCAN was trained in the supervised manner with HR images and synthetic LR images, which were generated by 3D nearest downsampling. Beware that degradation shift is introduced in this case, since the degradation from test LR images (with K -space truncation) is not the same as the one from training LR images.

As shown in Table I, UDEAN trained with both misaligned or unpaired LR and HR MRI images in unsupervised manner outperforms benchmarks 1 and 2 greatly in the metrics, and the Fig. 3 shows that the reconstructed SR images of benchmarks 1 and 2 are highly blurry, which are not applicable for clinical use. The benchmark 3 achieved better results than UDEAN in the metrics. However, due to the degradation shift between training and test LR images, the reconstructed SR image of benchmark 3 shown in Fig. 3 is over-smoothed, whereas the SR images of UDEAN delivered more detailed anatomical structures.

B. Comparison with the State-of-the-Art Unsupervised Methods

We also compare our proposed UDEAN with other state-of-the-art unsupervised methods, including ZSSR [9], CycleGAN [12], and DASR [14]. According to the numerical results in Table II, our UDEAN outperforms all the above mentioned methods greatly.

With unpaired HR and LR, the SSIM of our model is 0.008 and 0.031 higher than CycleGAN and DASR, respectively. The PSNR of our model is 1.19 dB higher than DASR and 0.46 dB lower than CycleGAN. With misaligned HR and LR, our model outperformed both CycleGAN and DASR with more than 0.025 in SSIM and 1.49 dB in PSNR.

Specifically, as shown in Fig.4, ZSSR generated highly blurry images, since the degradation representation between LR and HR MRI images could not be represented by using the learnt degradation representation between LR MRI images and lower resolution MRI images. Furthermore, since the

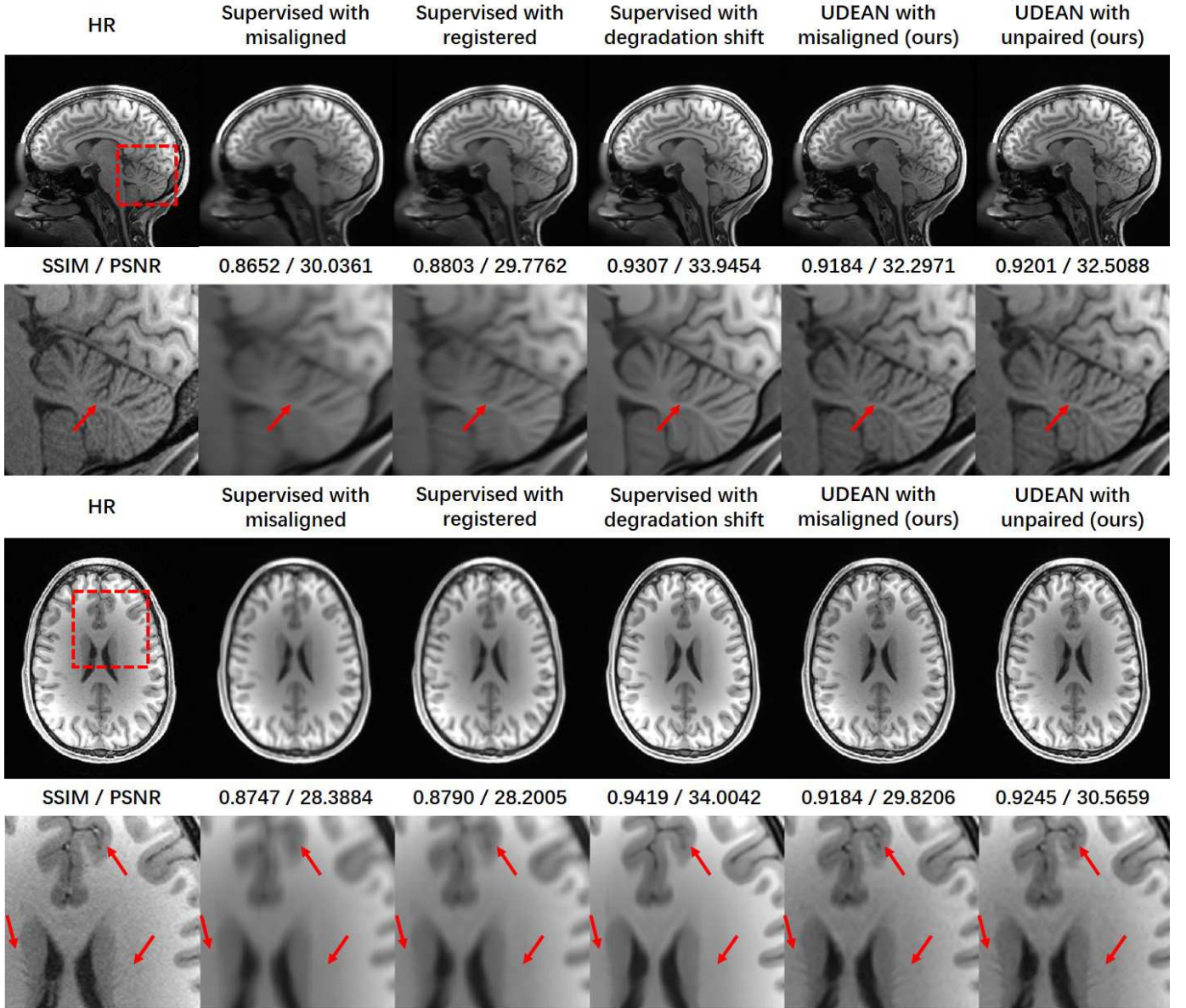


Fig. 3: Comparison of UDEAN with Supervised Methods for MRI SR with Geometric Deformation in Sagittal and Axial Plane.

TABLE II: Numerical Comparison of Different Unsupervised Methods for MRI SR with Upscale Factor of $2 \times 2 \times 2$, using Misaligned and Unpaired LR and HR Images

Method	SSIM	PSNR
Tricubic interpolation	0.8981 ± 0.0106	31.5862 ± 1.8520
ZSSR [9]	0.8984 ± 0.0158	32.5224 ± 2.0981
CycleGAN [12] with unpaired HR and LR	0.9164 ± 0.0080	33.9767 ± 1.7352
DASR [14] with unpaired HR and LR	0.8931 ± 0.0094	32.3309 ± 1.4671
UDEAN (ours) with unpaired HR and LR	0.9242 ± 0.0083	33.5159 ± 1.7234
CycleGAN [12] with misaligned HR and LR	0.8994 ± 0.0111	32.7870 ± 1.5203
DASR [14] with misaligned HR and LR	0.8946 ± 0.0091	32.2544 ± 1.4658
UDEAN (ours) with misaligned HR and LR	0.9247 ± 0.0097	34.2729 ± 1.8080

degradation representation between unpaired or misaligned HR and LR MRI images was not included, there were still evident errors on the boundaries of distinct soft tissues on the reconstructed SR MRI images, despite CycleGAN's high SSIM and PSNR. As the degradation representations between

unpaired or misaligned HR and LR MRI images were more complex for voxels on the boundaries of distinct soft tissues than the voxels inside the same soft tissue, utilizing CycleGAN reduced the geometric accuracy of boundaries of different soft tissues. Such geometric inaccuracy could result in inaccurate

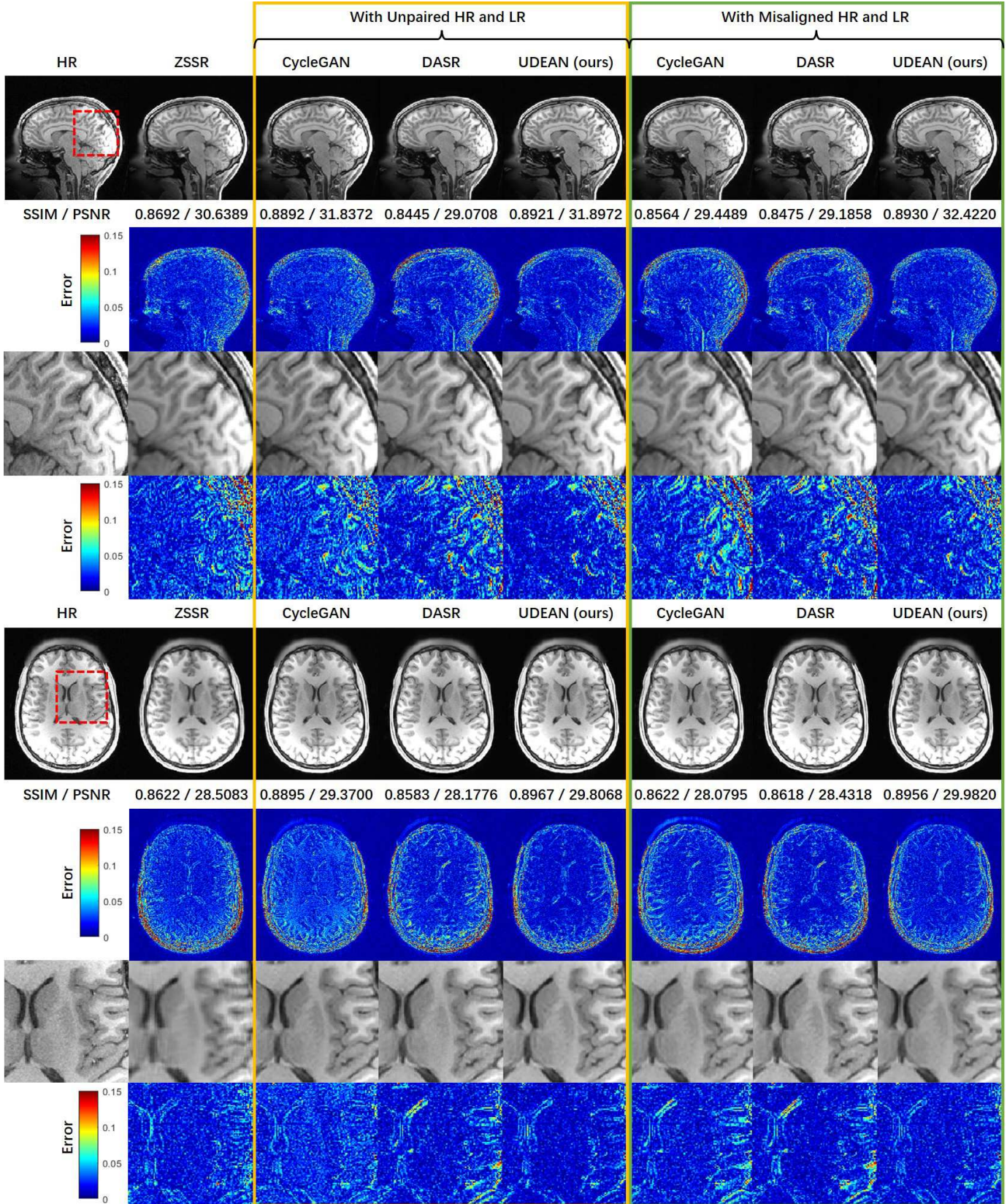


Fig. 4: Comparison of UDEAN with Other Unsupervised Methods in Visual Effect and Error Maps in Sagittal and Axial Plane.

surgery or therapy doses, indicating that the approach is not applicable in the real clinics. DASR, as the most recent unsupervised SR approach, learnt this degradation representation via a domain distance map, which it subsequently used to reconstruct SR MRI images. However, such learning was not under an end-to-end fashion, making this network difficult to be trained and learnt degradation representation hardly fit the reconstruction procedure. As a result, the inaccuracies in DASR's reconstructed SR MRI images are still massively visible. On contrast, our UDEAN adaptively learnt the degradation representation between the misaligned or unpaired LR and HR MRI images while applying it in the reconstruction with an end-to-end fashion, thus providing the minimum errors in the reconstructed MRI images.

IV. CONCLUSION

We propose the UDEAN as an unsupervised degradation adaption network that uses an end-to-end strategy to adaptively learn the degradation representation between misaligned or unpaired LR and HR MRI data. In real clinical settings, this network may alleviate the problem of lacking of paired authentic LR and HR images. Experimental results reveal that our model achieves enhanced image quality for SR reconstruction, and outperformed the state of the art methods.

REFERENCES

- [1] Pham, C. H., Ducournau, A., Fablet, R., Rousseau, F. (2017). Brain MRI super-resolution using deep 3D convolutional networks. IEEE 14th International Symposium on Biomedical Imaging (pp: 197-200)
- [2] Chen, Y., Xie, Y., Zhou, Z., Shi, F., Christodoulou, A. G., Li, D. (2018). Brain MRI super resolution using 3D deep densely connected neural networks. IEEE 15th International Symposium on Biomedical Imaging (ISBI).
- [3] Chen, Y., Shi, F., Christodoulou, A. G., Zhou, Z., Xie, Y., Li, D. (2018). Efficient and Accurate MRI Super-Resolution using a Generative Adversarial Network and 3D Multi-Level Densely Connected Network. International Conference on Medical Image Computing and Computer Assisted Intervention
- [4] Zhao, X., Zhang, Y., Zhang, T., Zou, X. (2019). Channel Splitting Network for Single MR Image Super-Resolution. IEEE Transactions on Image Processing (pp. 5649-5662)
- [5] Sui, Y., Afacan, O., Gholipour, A., Warfield, S. K. (2020, October). Learning a gradient guidance for spatially isotropic MRI super-resolution reconstruction. In International Conference on Medical Image Computing and Computer-Assisted Intervention (pp. 136-146). Springer, Cham.
- [6] Zhang, Y., Li, K., Li, K., Fu, Y. (2021). MR Image Super-Resolution with Squeeze and Excitation Reasoning Attention Network. In Proceedings of the IEEE/CVF Conference on Computer Vision and Pattern Recognition (pp. 13425-13434).
- [7] Feng, C. M., Fu, H., Yuan, S., Xu, Y. (2021, September). Multi-contrast mri super-resolution via a multi-stage integration network. In International Conference on Medical Image Computing and Computer-Assisted Intervention (pp. 140-149). Springer, Cham.
- [8] Li, H., Liu, J. (2021). 3D High-quality magnetic resonance image restoration in clinics using deep learning. arXiv preprint arXiv:2111.14259.
- [9] Shocher, A., Cohen, N., Irani, M. (2018). “Zero-shot” super-resolution using deep internal learning. In Proceedings of the IEEE conference on computer vision and pattern recognition (pp. 3118-3126).
- [10] Iwamoto, Y., Takeda, K., Li, Y., Shiino, A., Chen, Y. W. (2020). Unsupervised MRI Super-Resolution Using Deep External Learning and Guided Residual Dense Network with Multimodal Image Priors. arXiv preprint arXiv:2008.11921.
- [11] Cui, J., Gong, K., Han, P., Liu, H., Li, Q. (2022). Unsupervised arterial spin labeling image superresolution via multiscale generative adversarial network. Medical Physics, 49(4), 2373-2385.
- [12] Zhu, J. Y., Park, T., Isola, P., Efros, A. A. (2017). Unpaired image-to-image translation using cycle-consistent adversarial networks. In Proceedings of the IEEE international conference on computer vision (pp. 2223-2232).
- [13] Maeda, S. (2020). Unpaired image super-resolution using pseudo-supervision. In Proceedings of the IEEE/CVF Conference on Computer Vision and Pattern Recognition (pp. 291-300).
- [14] Wei, Y., Gu, S., Li, Y., Timofte, R., Jin, L., Song, H. (2021). Unsupervised real-world image super resolution via domain-distance aware training. In Proceedings of the IEEE/CVF Conference on Computer Vision and Pattern Recognition (pp. 13385-13394).
- [15] Sui, Y., Afacan, O., Gholipour, A., Warfield, S. K. (2021, September). MRI super-resolution through generative degradation learning. In International Conference on Medical Image Computing and Computer-Assisted Intervention (pp. 430-440). Springer, Cham.
- [16] Komninos, C., Pissas, T., Flores, B., Bloch, E., Vercauteren, T., Ourselin, S., Da Cruz, L., Bergeles, C. (2021, September). Intra-operative OCT (iOCT) Image Quality Enhancement: A Super-Resolution Approach Using High Quality iOCT 3D Scans. In International Workshop on Ophthalmic Medical Image Analysis (pp. 21-31). Springer, Cham.
- [17] Masutani, E. M., Bahrami, N., Hsiao, A. (2020). Deep Learning Single-Frame and Multiframe Super-Resolution for Cardiac MRI. Radiology (pp 192173)
- [18] Mao, X., Li, Q., Xie, H., Lau, R. Y., Wang, Z. (2016). Multi-class generative adversarial networks with the L2 loss function. arXiv preprint arXiv:1611.04076, 5, 00102.
- [19] Goodfellow, I., Pouget-Abadie, J., Mirza, M., Xu, B., Warde-Farley, D., Ozair, S., Courville, A., Bengio, Y. (2014). Generative adversarial nets. Advances in neural information processing systems, 27.
- [20] Van Essen, D. C., Smith, S. M., Barch, D. M., Behrens, T. E., Yacoub, E., Ugurbil, K., Wu-Minn HCP Consortium. (2013). The WU-Minn human connectome project: an overview. Neuroimage, 80, 62-79.
- [21] Zhang, Y., Li, K., Li, K., Wang, L., Zhong, B., Fu, Y. (2018). Image super-resolution using very deep residual channel attention networks. In Proceedings of the European conference on computer vision (ECCV) (pp. 286-301).
- [22] Lin, Z., Garg, P., Banerjee, A., Magid, S. A., Sun, D., Zhang, Y., Gool, L. V., Wei, D., Pfister, H. (2022). Revisiting RCAN: Improved training for image super-resolution. arXiv preprint arXiv:2201.11279.
- [23] Simonyan, K., Zisserman, A. (2014). Very deep convolutional networks for large-scale image recognition. arXiv preprint arXiv:1409.1556.
- [24] Wang, Z., Bovik, A. C., Sheikh, H. R., Simoncelli, E. P. (2004). Image quality assessment: from error visibility to structural similarity. IEEE transactions on image processing, 13(4), 600-612.
- [25] Huang, G., Liu, Z., Van Der Maaten, L., Weinberger, K. Q. (2017). Densely connected convolutional networks. In Proceedings of the IEEE conference on computer vision and pattern recognition (pp. 4700-4708).